High Activity Redox Catalysts Synthesized by Chemical Vapor Impregnation

Michael M. Forde,[†,§] Lokesh Kesavan,[†] Mohd Izham bin Saiman,[†] Qian He,[‡] Nikolaos Dimitratos,[†] Jose Antonio Lopez-Sanchez,[†] Robert L. Jenkins,[†] Stuart H. Taylor,[†] Christopher J. Kiely,[‡] and Graham J. Hutchings[†,*]

[†]Cardiff Catalysis Institute, School of Chemistry, Cardiff University, Main Building Park Place, Cardiff, CF10 3AT, United Kingdom, and and [‡]Department of Materials Science and Engineering, Lehigh University, 5 East Packer Avenue, Bethlehem, Pennsylvania 18015-3195, United States. [§]Present address: Department of Chemistry, University of the West Indies, St. Augustine Campus, Trinidad and Tobago.

ABSTRACT The use of precious metals in heterogeneous catalysis relies on the preparation of small nanoparticles that are stable under reaction conditions. To date, most conventional routes used to prepare noble metal nanoparticles have drawbacks related to surface contamination, particle agglomeration, and reproducibility restraints. We have prepared titania-supported palladium (Pd) and platinum (Pt) catalysts using a simplified vapor deposition technique termed chemical vapor impregnation (CVI) that can be performed in any standard chemical laboratory. These materials, composed of nanoparticles typically below 3 nm in size, show remarkable activity under mild conditions for oxidation and hydrogenation reactions of industrial importance. We demonstrate the preparation of bimetallic Pd—Pt homogeneous alloy nanoparticles by this new CVI method, which show synergistic effects in toluene oxidation. The versatility of our CVI methodology to be able to tailor the composition and morphology of supported nanoparticles in an easily accessible and scalable manner is further demonstrated by the synthesis of Pd_{shell}—Au_{core} nanoparticles using CVI deposition of Pd onto preformed Au nanoparticles supported on titania (prepared by sol immobilization) in addition to the presence of monometallic Au and Pd nanoparticles.

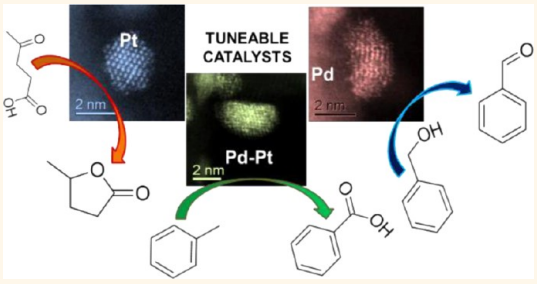

KEYWORDS: catalysis · bimetallic nanoparticle · nanoalloy · gold · palladium · platinum · core—shell structures · hydrogenation · oxidation

The application of nanoparticulate materials as heterogeneous catalysts is an attractive proposition when high selectivity to desired products needs to be coupled with high productivity and robust catalyst stability.[1] The high surface area-to-volume ratio of metal nanoparticles, which directly results from their very small particle size, can improve catalytic activity.[2,3] Recently, there have been many reports of highly active catalysts prepared by a number of liquid phase routes, *e.g.* sol-immobilization and electrochemical deposition, chosen specifically to afford supported metal nanoparticles with controlled size, composition, and dispersion.[4−7] Although these preparative routes are well established, it is often difficult in practice to control the physical dimensions and composition of supported metal nanoparticles.[8] For example, using sol-immobilization techniques, colloids containing nanoparticles with tunable size can generally be prepared for a wide number of metals and then deposited onto various supports. However, there are many parameters which influence the mean size of colloidal nanoparticles, (*e.g.*, varying the nature and concentration of stabilizer ligand, reaction volume, nature and concentration of the reducing agent, synthesis temperature/pressure/pH, solvent identity). This increases the complexity of applying a general protocol in the preparation of new materials in a systematic manner. Additionally, undesirable growth of the colloidal particles can occur, especially with aging in solution, or more commonly when the material is heat treated after deposition onto the support leading to inhomogeneities in the final material.[2] Furthermore, adsorption of the preformed colloidal nanoparticles onto a support surface may also cause the nanoparticle to restructure upon deposition and during subsequent heat

* Address correspondence to: hutch@cardiff.ac.uk.

Received for review November 5, 2013 and accepted December 16, 2013.

Published online December 16, 2013
10.1021/nn405757q

treatments.[9] These types of practical issues are not restricted to the sol-immobilization preparation alone, but also tend to complicate other liquid-phase catalyst preparation techniques (*e.g.*, coimpregnation, deposition, precipitation).

We set out to develop a new preparative method that circumvents the problem of surface contamination (*e.g.*, from protective stabilizer ligands in sol-immobilization, or from residual surface spectator species originating from the precursor salts in impregnation) which are inherent to liquid-phase preparation methods. To this end, we recognized that organometallic chemical vapor deposition (OMCVD) has been used previously to prepare thin metal films and also supported bimetallic nanoparticles (as powders), the latter usually utilizing a fluidized bed modification (FB-OMCVD).[10−16] The main advantages of vapor deposition methodologies include (i) improved purity of the deposited metal which is linked to the decomposition profile of the organometallic precursor and heat treatment conditions employed and (ii) a finer control over the particle/film characteristics of the deposited metal. Dry vapor methods can also facilitate high metal dispersion due to enhanced interaction (adsorption) between the organometallic precursor and support without surface modifiers.[11,16] Since the organometallic precursor is adsorbed onto the support without decomposition, it is reasonable to expect that the deposited metal sites are initially highly isolated and can potentially form very small nanoparticles upon heat treatment, especially in a reducing atmosphere. The lack of a preparation solvent also decreases the likelihood of surface contamination from residual solvent or the byproducts of solvent decomposition upon heat treatment. However, in terms of controlling the size, morphology, and composition characteristics of metal deposits using FB-OMCVD, there are a number of practical factors to consider which serve to increase the complexity of this method to the point where it firmly falls outside the usability range of most researchers that are interested in making supported metal nanoparticles for specific applications. These factors include the large amount of carrier gas required, extended deposition times, limitations in the use of supports which can be successfully fluidized, lack of control over the amount of deposited metal, temperature inhomogeneity in the system leading to contamination (from organic ligand decomposition products), among others.[11] Therefore, we aimed to develop a simplified version of the FB-OMCVD technique which reduces wastage of the organometallic precursor and does not require a carrier gas or fluidization of the support during the metal deposition step. We postulated that, given an appropriate choice of metal precursor, there is no fundamental reason why the metal precursor and support material could not be in direct physical contact with each other during the elevated temperature catalyst synthesis (comprising successive sublimation, deposition, and pyrolysis steps), as opposed to the conventional practice of having the precursor source physically remote from the substrate so as to separate the sublimation and deposition phenomenon. This idea has been recently demonstrated by Gallo *et al.*[17] and Papandrew *et al.*,[18] albeit with limited scope and characterization of the prepared materials, and is generally called a 'dry-mix' method. However, in most cases the resultant material is in the form of a thin films or larger nanoparticles, which is not the end goal of this current work.

We also considered that it should be possible to use our new approach to prepare bimetallic nanoparticles in a controlled manner by mixing two appropriate precursors prior to vapor impregnation or using a preformed material containing nanoparticles as a seed for the deposition of additional metals. Here we describe the successful preparation of highly active monometallic and bimetallic Pd and Pt heterogeneous catalysts supported on TiO_2 by our *chemical vapor impregnation* (CVI) method which follows on from our previous report of using this CVI technique for preparation of high activity Fe-loaded zeolite alkane oxidation catalysts.[19] The efficacy of the CVI method is demonstrated by the excellent catalytic activity of the resultant materials for three oxidation reactions, namely CO oxidation, solvent-free benzyl alcohol oxidation, and toluene oxidation.[20−23] We also present low-temperature levulinic acid hydrogenation, a potentially high value hydrogenation reaction that is linked to biorenewable energy and fuel research.[24−27] Finally, we conclude by demonstrating the potential of extending our technique to the synthesis of 'designer' nanoparticles with a core−shell architecture by using CVI to deposit a Pd shell onto pre-existing Au seed nanoparticles that were preformed by sol-immobilization methods and supported on titania.

RESULTS AND DISCUSSION

Catalyst Preparation and Structural Characterization. Our initial studies were inspired by the work of Sivakumar[28] and Dal Santo[15] who showed that it was possible to prepare nanoparticles on powdered supports using a "static" vapor deposition methodology. In our CVI version of this methodology (see Methods for full details) the precursor sublimation step and deposition onto the support are not spatially separated since the precursor and support are in intimate contact during the sublimation−deposition step. This is achieved by mixing high vapor pressure precursors with the support in a sealed Schlenk flask (or round-bottom flask) and heating at a temperature far below the decomposition temperature of the precursor under constant vacuum conditions (*i.e.*, $\sim 10^{-3}$ mbar) without the use of a carrier gas. It is important to note that careful choice of the temperature in the sublimation−deposition step is required to ensure that the metal precursor is

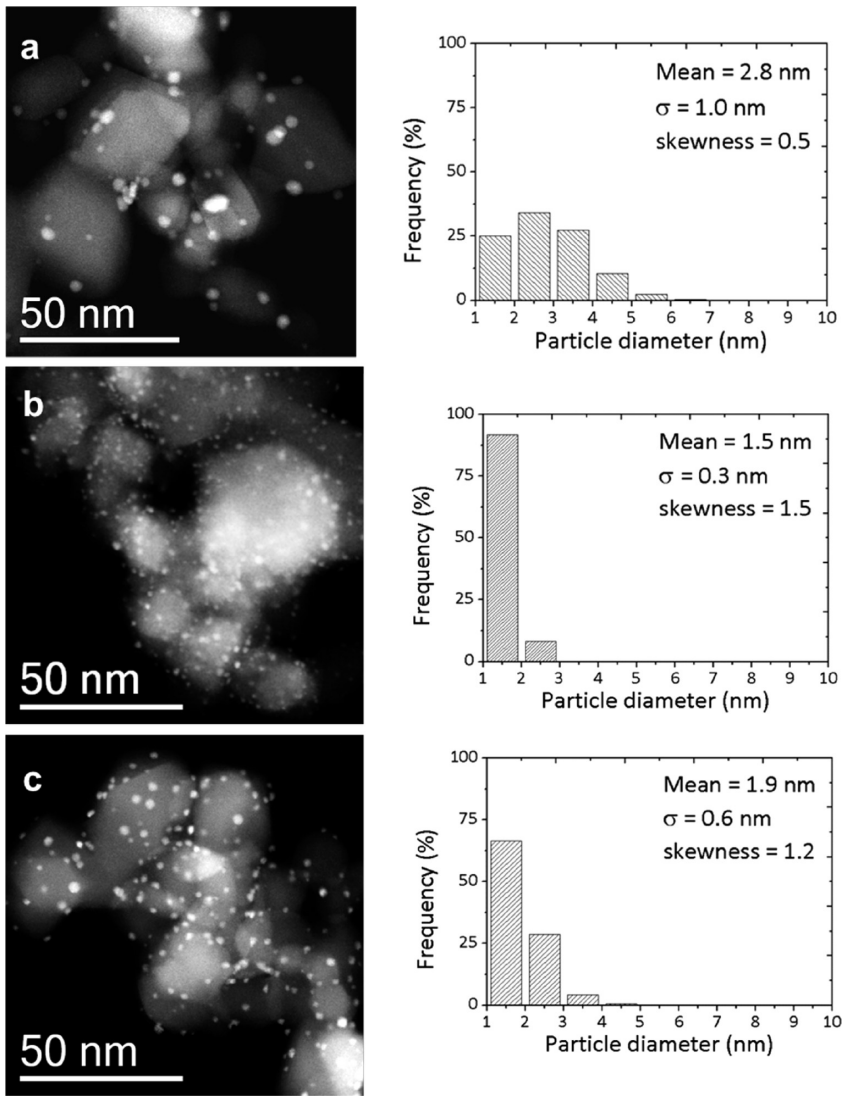

Figure 1. Representative low-magnification STEM-HAADF survey micrographs and the corresponding metal particle size distributions for (a) Pd/TiO_2, (b) Pt/TiO_2, and (c) $Pd-Pt/TiO_2$ samples prepared by the CVI route.

deposited (adsorbed) onto the support without decomposition. From a practical point of view, the preparation can be performed in any laboratory equipped with a standard vacuum pump and Schlenk line. Furthermore, the 'as-prepared' CVI material can be subsequently heat-treated under various atmospheres again using standard equipment. We chose metal acetylacetonate compounds as metal precursors due to their ease of handling and storage, wide availability in terms of the number of variants commercially available, and favorable sublimation characteristics.

We prepared TiO_2-supported Pd, Pt, and Pd–Pt catalysts and primarily characterized these materials using aberration-corrected scanning transmission electron microscopy (AC-STEM). High-angle annular dark field (HAADF) STEM imaging studies (Figure 1) confirmed that a uniform distribution of metal nanoparticles on the TiO_2 support was achieved with reasonably narrow size distributions, with mean particle sizes following the order Pt < Pt–Pd < Pd (1.5 nm, 1.9 and 2.8 nm, respectively). We also noted the presence of a significant quantity of subnanometer clusters and isolated atoms that are marked with white arrows in higher-magnification HAADF images presented in Figure 2a and Figure S1 in Supporting Information (SI). The existence of these subnanometer entities are remarkable, considering the high-temperature reduction treatment (in 5% H_2/Ar at 400 °C) used during the final stage of the preparation. Reflecting on our previous work with sol-immobilization and impregnation catalysts where we observed extensive particle growth if the material was heat treated above 200 °C,[20,21,29] we note that such sintering behavior is apparently not problematic using this new CVI technique. Additionally, bright field-STEM (BF-STEM) images of particles in profile view showed little evidence of amorphous carbon deposits (which could originate from the decomposition of organic moieties of the organometallic

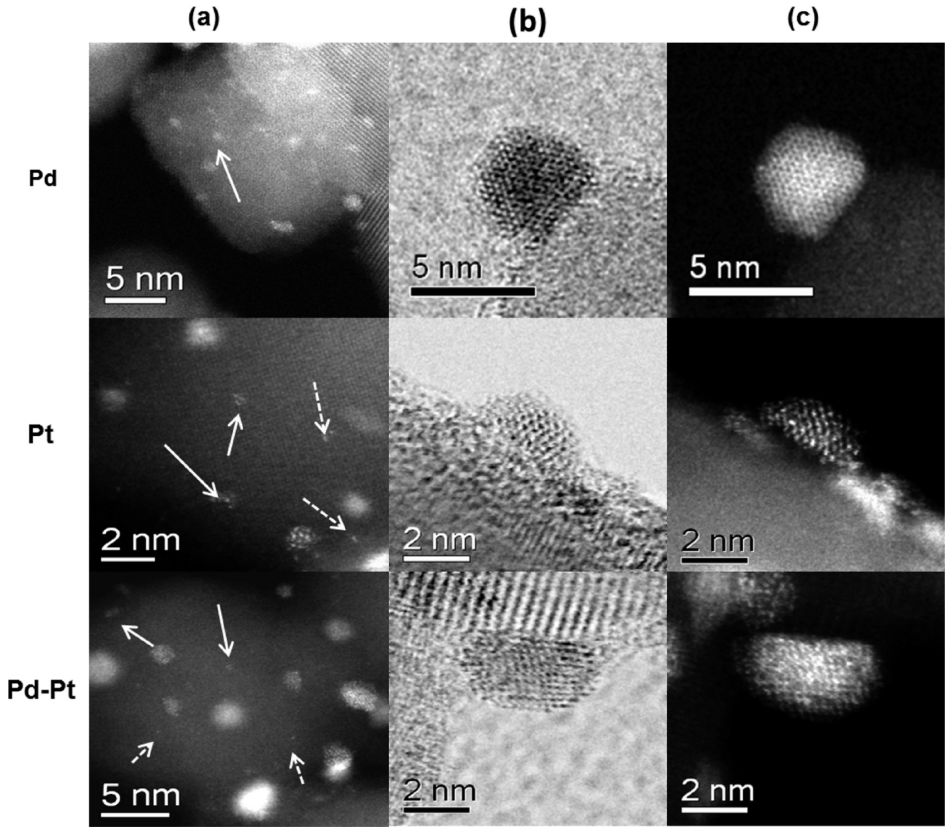

Figure 2. (a) Representative STEM-HAADF images and complementary (b) BF-STEM and (c) HAADF-STEM pairs of individual particles in the 2.5 wt % Pd/TiO_2 (*top row*), 2.5 wt % Pt/TiO_2 (*middle row*), and 1.25 wt % Pd−1.25 wt % Pt/TiO_2 (*bottom row*) CVI catalysts. Solid white arrows indicate faint subnanometer clusters and dashed white arrows in (a) show isolated atoms present on the TiO_2 support material. The BF-STEM profile images in column (b) show crystalline nanoparticles with clean surfaces which are characteristic of the entire sample. All catalysts were reduced for 3 h at 400 °C under a 5% H_2/Ar flow.

TABLE 1. Summary of XPS, STEM, ICP and CHN analysis of the Pd, Pt, and Pd−Pt catalysts supported on TiO_2 prepared by the chemical vapor impregnation method

catalyst	mean particle size (nm)[a]	binding energy (eV)[b]	oxidation state[b]	actual metal loading wt %[c]	CHN analysis
2.5 wt % Pd/TiO_2	2.8 ± 1.0	Pd(3d) 334.6	metallic	2.12	0.26 wt % C, 0.09 wt % H
2.5 wt % Pt/TiO_2	1.5 ± 0.3	Pt(4f) 70.7	metallic	1.72	0.12 wt % C, 0.04 wt % H
1.25 wt % Pd−1.25 wt % Pt/TiO_2	1.9 ± 0.6	Pd(3d) 334.9	metallic	Pd 1.26	0.04 wt % C, 0.02 wt % H
		Pt(4f) 70.5		Pt 1.18	

[a] Measured from multiple HAADF-STEM images. [b] Measured by XPS. Binding energy referenced against C 1s = 284.7 eV. [c] Measured by ICP-MS.

precursor) on the nanoparticle surfaces (Figure 2b). However, to investigate further the possibility of carbon deposits (*i.e.*, not necessarily on the metal nanoparticle surfaces) after pyrolysis we performed carbon−hydrogen−nitrogen (CHN) analysis on the materials. Carbon was found on the Pd-only and the Pt-only catalysts (0.26 wt % and 0.12 wt %, respectively, Table 1). The higher amount of carbon on the surface of the Pd-only catalyst may be due to the low-temperature autoreduction of the metal precursor which occurs during the synthesis in the absence of H_2 (see Methods). The bimetallic Pd−Pt material showed virtually no carbon deposited on the surface, even though it was heat treated under exactly the same conditions as the monometallic materials. The reason for the negligible carbon contamination in the bimetallic catalyst is unknown, and further investigation of this phenomenon is underway. However, these data point to the beneficial effect of mixing the two metal precursors to achieve a catalyst that is relatively free of undesirable carbon contamination.

We had a special interest in the structure of the 1.25 wt % Pd−1.25 wt % Pt/TiO_2 CVI sample, as it was previously shown that randomly alloyed or tailored core−shell nanostructures could be accessed by varying the catalyst preparation methodology (*e.g.*, using a different sequence of metal addition/reduction steps in sol-immobilization).[21,22] Bimetallic nanoparticles are now being employed in many fields including catalysis, drug delivery, biomedical and pharmaceutical applications,

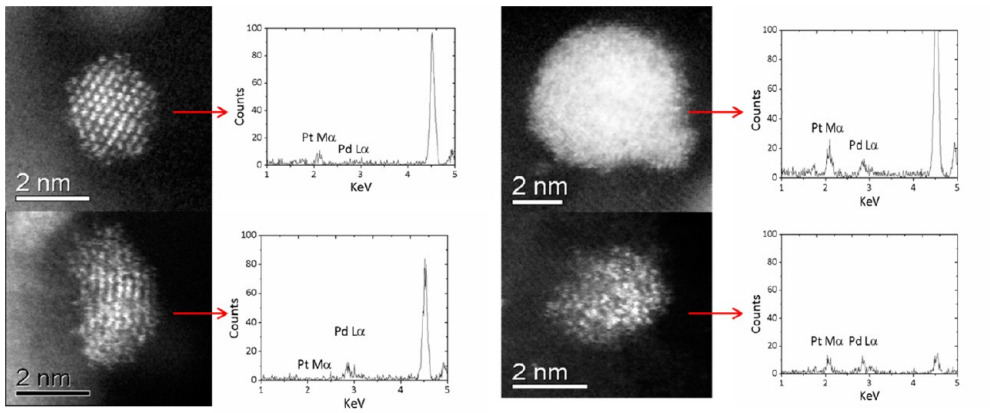

Figure 3. XEDS analysis of individual particles in the 1.25 wt % Pd−1.25 wt % Pt/TiO_2 material prepared by CVI. The composition of the metal particles was found to be quite variable: *e.g.* very Pt-rich (*top left*), very Pd-rich (*bottom left*), and mixed alloys of Pt + Pd (*top right and bottom right*). The Pt−Pd mixed-alloy nanoparticles were by far the dominant species observed. The nature of the subnanometer clusters and individual atoms as present in this sample could not be determined as these entities were too small for XEDS analysis.

imaging, and related applications.[30] In the field of catalysis, it is known that the morphology of bimetallic particles play an important role in their catalytic properties.[7,31,32] For example, Strasser and co-workers[33] recently commented on the improved stability and catalytic activity of many Pt-based core−shell nanoparticles over their Pt only analogues used in fuel cell applications. This is not a restricted case as other researchers have shown the beneficial effects of different bimetallic particle configurations for a range of reactions as given in recent reviews,[27,30,33] with effort now being put into the synthesis of trimetallic core−shell nanoparticles.[32] X-ray energy dispersive spectroscopy (XEDS) analysis of individual nanoparticles in our 1.25 wt % Pd−1.25 wt % Pt/TiO_2 sample revealed that the vast majority of them are random Pd−Pt alloys of variable composition, along with very occasional non-alloyed monometallic Pd and Pt particles (Figure 3). In this case, core−shell structured nanoparticles were not observed (or expected) as we were just using a one-step deposition technique. Furthermore, XPS analysis (Table 1) of the freshly prepared materials showed that the Pd and Pt components were in the metallic state in all the fresh catalysts. However, BF-STEM imaging of Pd-containing samples that had been aged over the time frame of 6 months under ambient storage conditions showed distinct amorphous surface regions that could be indicative of the formation of an oxide layer on the nanoparticles (Figure S2 SI), but these materials were still active for oxidation reactions such as benzyl alcohol oxidation. We should point out that the observation of thin oxide layers by HAADF-STEM in the fresh catalyst would not be possible using our current techniques, and so we cannot rule out the presence of ultrathin oxide layers in the freshly prepared catalyst.

Since our interest in bimetallic nanoparticles includes nanoparticles having core shell morphologies, we have also utilized a preformed sol-immobilized material composed of Au nanoparticles on TiO_2 as the "support" followed by the deposition of a second metal by CVI to demonstrate the wider applicability of the methodology and to illustrate the possibility of deliberately forming core−shell structures. A 1 wt % Au/TiO_2 material was prepared by sol-immobilization and refluxed as described in our previous work.[29] This material was dried at 110 °C for 16 h and then ground in an agate mortar and pestle before the deposition of $Pd(acac)_2$ using the CVI method. Figure 4 shows representative STEM data from this hybrid CVI/sol-immobilized Au−Pd/TiO_2 material where some particles having a definite Pd_{shell}−Au_{core} morphology were formed as expected (see the *z*-contrast imaging and XEDS data in b, c, and d of Figure 4, respectively). Additionally, a significant population of secondary 2 nm Pd particles and subnanometer Pd clusters were also nucleated on the support as indicated with green arrows in Figure 4b, and it was possible to still find some Au particles which had not been coated with a Pd shell as highlighted with yellow arrows in Figure 4b. However, we note that the images shown in a and b of Figure 4 are representative of the relative proportions of Pd_{shell}−Au_{core}, Au-only, and Pd-only particles in the sample as a whole, and as such the latter species do not dominate on the titania surface. Although more work is undoubtedly still needed to perfect the technique, our preparation of at least some Pd_{shell}−Au_{core} particles by this hybrid sol-immobilization/CVI method is an important and encouraging advance as it expands the potential versatility and scope of the CVI synthesis method. The ability to modify preformed or commercial catalysts by the controlled and selective CVI deposition of additional metals would open up a plethora of novel catalyst design possibilities.

Catalysis Using Supported Nanoparticles Prepared by CVI. *CO Oxidation Studies.* Initially, we investigated the oxidation of CO, which is a highly structure-sensitive

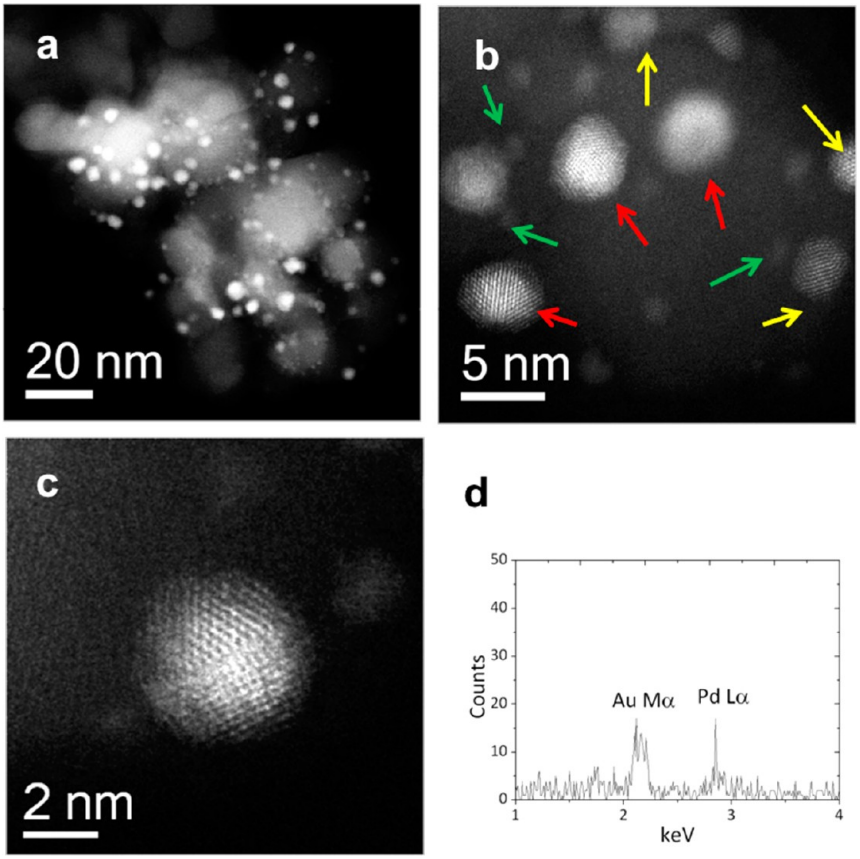

Figure 4. Representative STEM-HAADF images of Au−Pd/TiO_2 catalysts prepared *via* the hybrid CVI/sol-immobilization method; (a) a low magnification HAADF survey image; (b) higher magnification HAADF micrograph showing some Pd_{shell}−Au_{core} nanoparticles (highlighted with red arrows) as well as some monometallic Au particles that were uncoated (yellow arrows) and monometallic Pd particles (green arrows); (c) a HAADF image of a Pd_{shell}−Au_{core} nanoparticle and its corresponding XEDS spectrum (d) confirming the coexistence of both and Au and Pd.

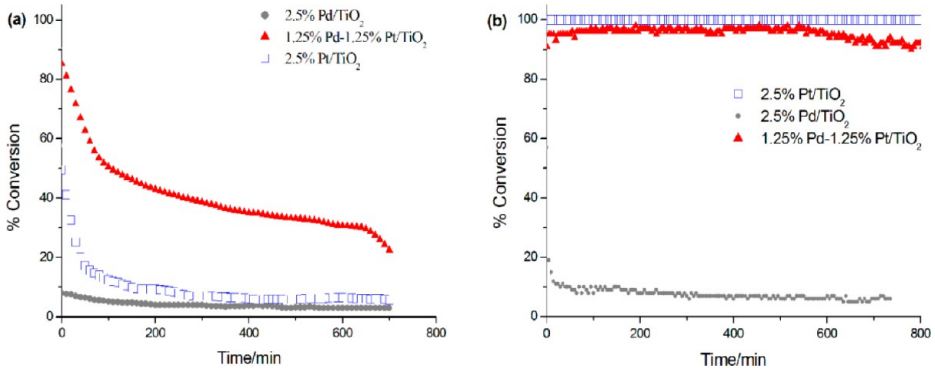

Figure 5. CO oxidation results at (a) 25 °C and (b) 50 °C for 2.5% Pt/TiO_2 (gray filled circles), 2.5% Pd/TiO_2 (open blue squares), and 1.25% Pd−1.25% Pt/TiO_2 (filled red triangles). The loadings given are nominal values based on the mass of precursor used in catalyst preparation. Reaction *conditions:* 50 mg catalyst, 21 mL min^{-1}, 5000 ppm CO/air, GHSV 25,200 mL g $(cat)^{-1}$ h^{-1}.

reaction, (dependent on particle size and shape as well as oxidation state of the metal)[34] using the reduced Pd−Pt/TiO_2 CVI catalysts at 25 °C and 0.5% CO in an air/gas feed. Under these conditions the most active catalyst was the bimetallic 1.25 wt % Pd−1.25 wt % Pt/TiO_2 material followed by the monometallic 2.5 wt % Pt/TiO_2 and then 2.5 wt % Pd/TiO_2 samples (Figure 5). It is noteworthy that the addition of Pt to Pd improved both the conversion and stability of the catalysts since deactivation was noted for all samples but was much less pronounced for the bimetallic Pd−Pt material (see Figure 5a). The same series of catalysts were then studied for the same reaction at higher temperature (50 °C). By increasing the temperature from 25 to 50 °C, a significant increase of activity was observed, with both the 2.5 wt % Pt/TiO_2 and 1.25 wt % Pd−1.25 wt % Pt/TiO_2 catalysts showing enhanced conversions of 90−100%. It is important to

emphasize that the catalyst deactivation rate was decreased by increasing the reaction temperature, and in the case of the 2.5 wt % Pt/TiO_2 material, the same conversion was maintained throughout a prolonged reaction period (24 h), thus demonstrating a high degree of stability under these conditions. If the 2.5 wt % Pt/TiO_2 catalyst was placed in a flowing nitrogen atmosphere for 4 h at room temperature after deactivation was observed and then retested for CO oxidation at 25 or 50 °C, the catalytic performance reverted to that observed in the initial run. This suggests that deactivation was not due to any gross changes in the nanoparticles themselves (*e.g.* particle sintering or redispersion of the metal), and in principle deactivation could be caused by the blocking of active sites through the formation of carbonate species on the surface of the metal particles.[35,36] Increasing the reaction temperature may mitigate this deactivation effect by the continuous removal of carbonate species from the catalyst surface.[37,38] Generally, CO oxidation using supported Pt catalysts is conducted at higher temperatures (>100 °C) for appreciable conversion to be observed,[37−40] and thus further direct comparison of our materials is difficult. However, we note here that the activity of the CVI 2.5 wt % Pt/TiO_2 sample at 50 °C (16.5 mmol CO mol $^{-1}$ Pt s^{-1}) is significantly higher than the counterpart Pt/TiO_2 materials (0.03 mmol CO mol $^{-1}$ Pt s^{-1}) prepared by conventional wet preparation methods.[41] The performance of the CVI material is also comparable to other Pt/Al_2O_3 and Pt/FeO_x catalysts prepared by colloidal methods when used at a similar reaction temperature of 25−50 °C (1−6 mmol CO mol $^{-1}$ Pt s^{-1}).[37,38] For those latter Pt-containing materials, the oxide supports have been shown to have a promoting effect on the catalysis, and the presence of a substantial amount of water vapor in the reactant gas feed is essential in order to achieve high activity under mild conditions.[37,38] In related work Pt nanoparticles encapsulated in hollow CeO_2 fibers have been used for CO oxidation but the high TOF reported was based on the amount of surface Pt sites (not overall Pt loading).[42]

Benzyl Alcohol Oxidation. We investigated the oxidation of benzyl alcohol with O_2 as oxidant, since the oxidation products of the benzyl alcohol (*i.e.*, benzaldehyde, benzoic acid, and benzyl benzoate)[20,43] are all important materials in the chemical industry. With our Pd/TiO_2 CVI catalyst we observed high activity for benzyl alcohol oxidation with TOF values in excess of ≥12000 h^{-1} (Figure 6a) which we consider is due to a combination of the very small Pd particle size (2.8 ± 1.0 nm) and its metallic oxidation state. Introduction of Pt into the Pd catalyst resulted in lower catalytic activity, with TOF values in the 6000−9000 h^{-1} range. Nevertheless, Pt had a positive influence on the distribution of products, because a decrease in the selectivity to toluene and a corresponding enhancement in

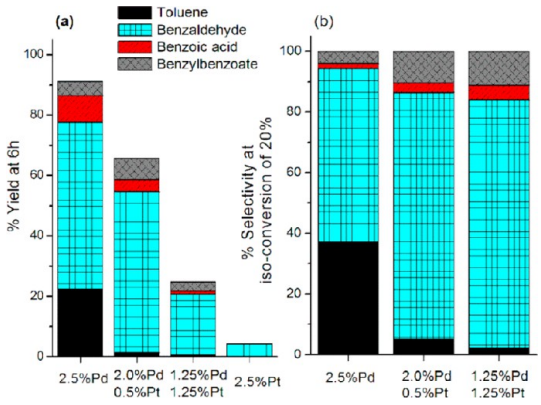

Figure 6. Oxidation of benzyl alcohol with O_2 as oxidant using titania-supported Pd/Pt catalysts with 2.5 wt % total metal content but varying composition prepared by CVI. (a) Product yield at 6 h reaction time and (b) comparison of selectivity at iso-conversion level of 20%. *Key:* Solid black - toluene; blue plaid - benzaldehyde; red diagonal lines- benzoic acid; gray cross-hatched - benzyl benzoate.

benzaldehyde selectivity was observed. This is further demonstrated by comparison of the Pd−Pt catalysts at an iso-conversion level of 20% (Figure 6b), where toluene selectivity decreased from 37% to 2−5% by incorporating Pt, while benzaldehyde selectivity increased from 57% to 82%. This effect was evident even for low levels of Pt (0.5 wt %) added to the Pd/TiO_2 catalyst (Table S1 SI). Toluene could be formed by either disproportionation or hydrogenolysis of benzyl alcohol, and both pathways require surface hydrogen. In this reaction, surface-adsorbed hydrogen may be derived from dehydrogenation of the C−OH moiety in benzyl alcohol and is probably present in the form of metal hydrides. Pd is known to catalyze the formation of toluene,[21] and we have shown that careful tuning of the surface-exposed Pd content in bimetallic Au−Pd catalysts[21,22,43] or, more recently, the addition of a minute amount of Pt to Au−Pd catalysts greatly decreases the formation of toluene.[44] Considering that Pt−H is more stable than Pd−H (~330 ± 30 *vs* 234 ± 25 kJ mol^{-1}[45]), one may rationalize the observed effect for Pt in terms of lowering the ability of the nanoparticles (which are present as random alloys) to execute the hydrogen transfer reaction, if Pd is the more active component for the overall oxidation pathway.

We note that controlling the selectivity to benzaldehyde is crucial for industrial applications and that our new CVI catalysts showed high activity as compared to other Pd−Pt[46] and Au−Pd[20,22] materials prepared by sol-immobilization and impregnation (see Table S2 SI).

Toluene Oxidation. The selective oxidation of toluene is a challenging reaction due to the high C−H dissociation bond energy and low polarizability of the alkyl moiety. We have previously demonstrated that Au−Pd nanoparticles in the 3−5 nm size range (prepared by sol-immobilization methods) are highly active for the solvent-free oxidation of toluene using

molecular oxygen at 160 °C or TBHP at 80 °C as oxidants.[9] Conversion levels of 99% could be achieved, while maintaining a selectivity of 95% toward benzyl benzoate[9] using this catalytic system (O_2 as oxidant) which operates under conditions where noncatalytic autooxidation reactions are minimized. Our new series of CVI-derived Pd−Pt catalysts were tested for toluene oxidation, and the catalytic data are presented in Figure 7 and Figure 8. The most active catalyst for the solvent-free liquid-phase oxidation of toluene was the bimetallic 1.25 wt % Pd−1.25 wt % Pt/TiO_2 system, followed by the monometallic Pt/TiO_2 and Pd/TiO_2 catalysts (Figure 7). It should be noted, however, that the use of Pd−Pt alloys enhanced the formation of benzoic acid instead of benzyl benzoate, which in this case is clearly linked to the presence of Pt in the material as the monometallic Pt/TiO_2 catalysts also showed appreciable benzoic acid selectivity as compared to that shown by the Pd/TiO_2 material (Figure 7). These data are an interesting contrast to the case of Au−Pd/TiO_2 catalysts where benzyl benzoate was always the major product.[9] Therefore, this new generation of catalysts allows further tuning of the product distribution to selectively afford benzoic acid, which is also a key industrial chemical. Additionally, a synergistic effect on conversion was observed in the case of the bimetallic Pd−Pt material which prompted us to investigate the possibility of achieving even higher conversion levels. Under modified conditions, *i.e.* a lower substrate/metal molar ratio, a 99% conversion level with a concomitant 91% selectivity to benzoic acid was achieved after 96 h (Figure 8a). An interesting feature of the time-online analysis shown in Figure 8a is that after 24 h a switch of the product distribution from favoring benzyl benzoate to benzoic acid occurred which may indicate some change in the active sites of the catalyst. However, we also note that this high degree of activity is comparable that that achieved with our most active random alloy Au−Pd-supported catalysts synthesized by colloidal methods,[9] but with a different major product, *i.e.*, benzoic acid instead of benzyl benzoate.

We also attempted the oxidation of toluene using *tert*-butyl hydroperoxide (TBHP) as oxidant at a lower temperature (80 °C). Under conditions analogous to those we have used in previous studies,[23] we found that our Pd−Pt/TiO_2 CVI catalyst showed high conversion of toluene with benzoic acid being the major product. In this case, the product distribution leans toward benzoic acid as opposed to benzyl benzoate due to the influence of the choice of oxidant, as we have previously shown.[23,46] The key data from this series of reactions are found by examining the TBHP conversion as the reaction proceeds. The TBHP conversion begins to level off after 24 h, but the oxidation of toluene continues. This finding is in stark contrast to our reports of Au−Pd/TiO_2 catalysts (prepared by sol-immobilization)[23] employed in this reaction, where the TBHP conversion remained double that of the toluene conversion throughout the reaction. Additionally, a 0.5 wt % Pd−0.5 wt % Pt/TiO_2 catalyst (prepared by sol-immobilization) was tested in the oxidation of toluene using TBHP, and we found nearly complete decomposition of TBHP and low catalytic activity.[46] These data highlight the advantage of preparing small nanoparticles in the absence of stabilizing ligands that can potentially block metal sites. By considering the quantity of oxygen present in the products *vs* oxygen available from TBHP, we found ~3.3 times excess in the products with our CVI material. This finding is compounded by the known decomposition pathways of TBHP[47] which show that *tert*-butanol is a major primary product (as well as its alcohol cleavage products), thereby indicating that only one oxygen atom from the TBHP molecule is actually found in the primary hydrocarbon oxidation products. Thus, our data strongly suggest the activation and incorporation of oxygen from the air (since the reaction was done under an air atmosphere) with TBHP acting as an initiator and not as a stoichiometric oxidant. One may attempt to explain these data by considering the autocatalytic effect of benzaldehyde which is present in appreciable amounts (~8−16% toluene conversion with 18−30% benzaldeyhde selectivity) at the shorter reaction times (24−48 h). However, our previous work using sol-immobilized Au−Pd/TiO_2 material also showed appreciable conversion and benzyaldehdye selectivity at 24 h (18% and 25%, respectively), but the TBHP conversion remained double that of the toluene conversion as the reaction proceeded,[23] indicating that benzaldehyde was playing no major catalytic role in the activation of toluene and oxygen under these conditions. If the reaction mixture was left at room temperature (20 °C) in air with stirring for an extended period (3 weeks), we found that the reaction vessel contained solidified benzoic acid and that toluene had

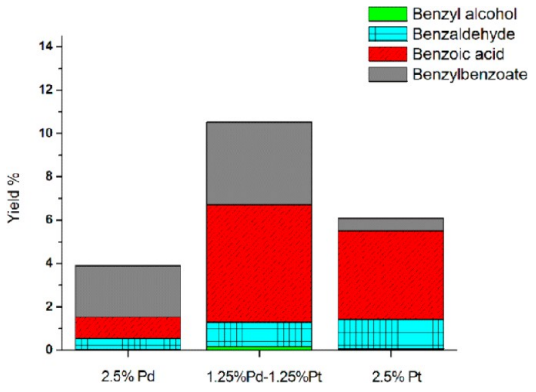

Figure 7. Comparison of the catalytic activity of TiO_2-supported Pd and Pt CVI catalysts in the oxidation of toluene under solvent-free conditions at 160 °C using molecular O_2. *Key:* Solid black - toluene; blue plaid - benzaldehyde; red diagonal lines - benzoic acid; gray cross-hatched - benzyl benzoate.

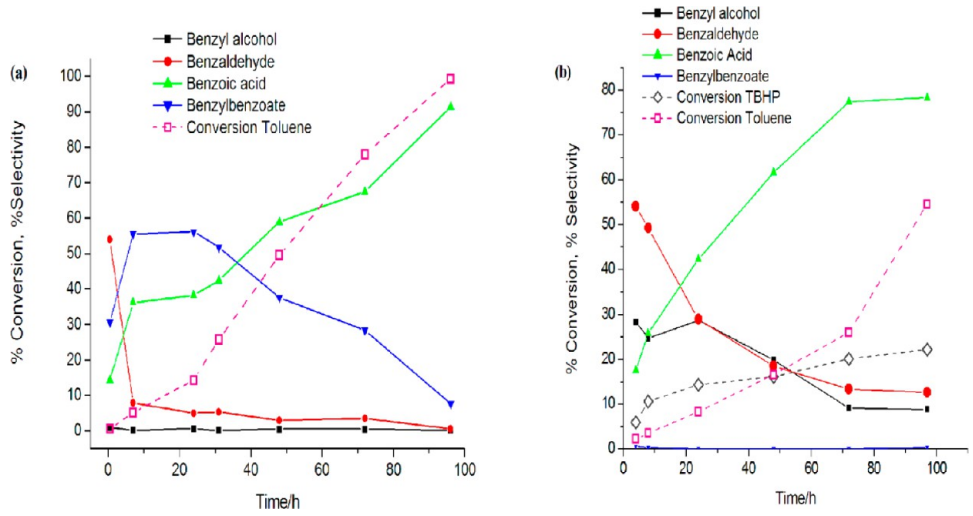

Figure 8. Catalytic activity of 1.25% Pd−1.25% Pt/TiO_2 prepared by CVI for the solvent-free oxidation of toluene at (a) 160 °C using O_2 and (b) 80 °C using TBHP. *Key:* Black line with filled square marker - benzyl alcohol; red line with filled circle marker - benzaldehdye; green line with green upward triangle marker - benzoic acid; blue line with filled downward triangle marker - benzylbenzoate; dashed black line with open diamond marker - conversion of TBHP; dashed pink line with open square marker - conversion of toluene.

undergone complete conversion. Considering the relatively low availability of molecular oxygen (from ambient air) and the very mild reaction temperature employed, we do not consider our data to be the result of autooxidation involving benzaldehyde, but instead require the involvement of bimetallic Pd−Pt particles in the activation of molecular oxygen and toluene. To the best of our knowledge, this is the first report showing such exceptional activity for supported Pd−Pt catalysts for these reactions, and also the first demonstration of the low-temperature activation of molecular oxygen by this Pd−Pt/TiO_2 system in the oxidation of C−H bonds.

Hydrogenation of Levulinic Acid. Noting that Pt and Pd have also previously been employed as hydrogenation catalysts, we postulated that our materials should also show high hydrogenation activity. We chose the hydrogenation of levulinic acid (LA) to γ-valerolactone (GVL) as a test reaction, because the former is poised to become a readily accessible biorefinery raw material which can be converted to high-value products.[24] Levulinic acid is a biorenewable platform chemical that can be economically derived from lignocellulose found in nonfood crops or agricultural waste and hydrogenated to γ-valerolactone (GVL), valeric acid (VA), 1,4-pentanediol (1,4-PDO), methyl tetrahydrofuran (MTHF), and others (see Scheme 1). Each of these hydrogenation products can be used as fuel additives (directly, or as higher-molecular weight esters in the case of valeric acid)[48] or in the production of precursors for chemicals and plastics.[26,27,48] Near-quantitative LA conversion under high-temperature hydrogenation conditions (typically >220 °C, 40 bar H_2, H_2/LA > 4) has already been reported;[26,41,48−50] therefore, we

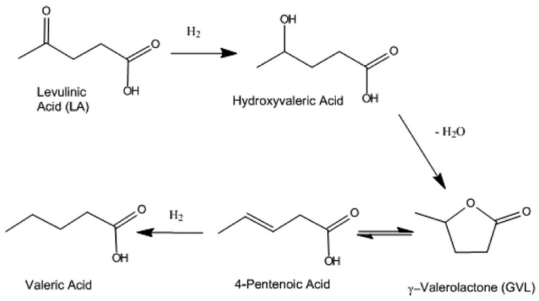

Scheme 1. Hydrogenation of levulinic acid to γ-valerolactone

decided to attempt the reaction under much milder conditions, considering the high catalytic activity we observed for our CVI-derived materials in other reactions. We found that using our Pt/TiO_2 CVI material, a 10 wt % aqueous solution of LA acid could be completely hydrogenated to GVL with only very minor amounts of other products being generated at 100 °C with a TOF of 336 mol product mol(Pt)$^{-1}$ h^{-1} (Table 2, and Figures S2, S3 in SI). These data compare favorably with other reports,[48] as in our case the hydrogenation temperature is much milder (see Table S3 in SI for typical reference data for comparison). The 1.25 wt % Pd−1.25 wt % Pt/TiO_2 and 2.5 wt % Pd/TiO_2 variants did not show the same level of activity under these very mild reaction conditions but were able to achieve high conversion of LA at 150 and 210 °C, respectively (Table 2). We decided to increase the amount of substrate to a 50 wt % aqueous solution of levulinic acid and also observed almost complete conversion at only 150 °C (TOF of 480 h^{-1}, Table 2) using the Pt/TiO_2 catalyst. Interestingly, we found that a H_2/LA ratio of 1 could be employed even with these more concentrated solutions of LA indicating near

TABLE 2. Hydrogenation of aqueous phase levulinic acid (LA) using Pd−Pt/TiO_2 catalysts prepared by the CVI method[a]

				selectivity %[b]					
catalyst	*T*/°C	*t*/h	conversion%	GVL	hydroxy valeric acid	4-pentenoic acid	valeric acid	others	TOF[c]
2.5% Pt/TiO_2	100	4	100	97.1	2.9	—	—	—	336.0
1.25% Pd— 1.25% Pt/TiO_2	100	4	44.4	93.1	2.5	3.8	1.6	—	104.2
1.25% Pd— 1.25% Pt/TiO_2	150	4	92.5	95.6	3.1	0.7	—	0.6	222.6
2.5% Pd/TiO_2	100	4	2.1	89	—	11	—	—	15.1
2.5% Pd/TiO_2	210	4	90	96.6	2.5	—	0.2	0.7	164.9
2.5% Pt/TiO_2	30	20	57.5	66.2	33.8	—	—	—	38.6
2.5% Pt/TiO_2[d]	150	7	100	98.3	1.7	—	—	—	480.0

[a] *Test conditions:* catalyst mass: 0.05 g; reaction volume: 10 mL; [LA]: 10 wt %; H_2/LA = 3.6; stirring rate 1200 rpm; P(H_2): 30 bar. [b] Selectivity calculated as mol C5 product/total moles C5 products. [c] Calculated as mol LA acid converted/ (mol metal × time (h)). [d] [LA]: 50 wt %; reaction volume: 10 mL; catalyst mass: 0.1 g; H_2/LA= 1.0; stirring rate: 1200 rpm.

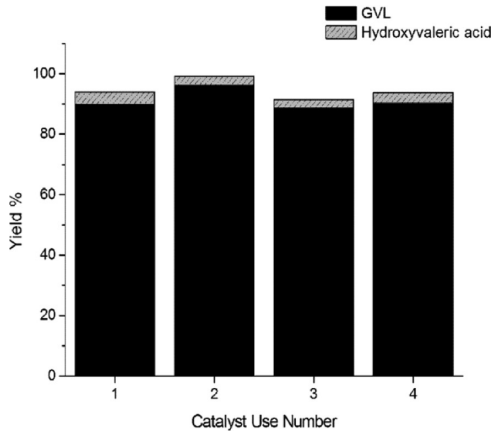

Figure 9. Reusability testing of a 1.72 wt % Pt/TiO_2 CVI catalyst for levulinic acid hydrogenation over four cycles in a batch reactor. *Test conditions*: 10 wt % levulinic acid aqueous solution (20 or 40 mL); time: 5 h, reaction temperature: 150 °C, stirring rate: 1200 rpm; *P*(H_2) 30 bar or 50 bar; catalyst mass: 100 mg or 200 mg, reactor internal volume: 70 mL. Catalyst was recovered by filtration under vacuum followed by drying in a N_2 stream at 90 °C for 1 h prior to reuse. The metal:substrate ratio was kept constant at 19:98.

quantitative utilization of hydrogen (with additional positive pressure being supplied by an inert gas in the reactor), which is in contrast to the usual requirement of H_2/LA > 4 reported for this reaction.[26,48] Importantly, the Pt/TiO_2 catalyst was also reused over four reaction cycles in a larger reactor with an adjustment of the volume of levulinic acid solution and catalyst amount (Figure 9), and similar results were found in each test, indicating that the catalyst was stable under reaction conditions without a regeneration step (*i.e.*, without heat treatment in H_2 between runs).

CONCLUSIONS

We have demonstrated that the simplicity of our initial mixing approach and careful choice of conditions to afford small nanoparticles (<4 nm) is a key advantage of the method over the FB-OMCVD technique, as it obviates the need for complex equipment. It is also important to emphasize that the formation of large agglomerated nanoparticles can be readily avoided using this CVI technique even following the relatively high-temperature treatment of the catalysts, and the surface of the material is relatively free of residual carbon contamination. The presence of subnanometer particles in our new materials, even after harsh catalyst treatments, also suggests that the methodology may afford an opportunity to study catalytic reactions on subnanometer particles in more realistic catalytic systems. Furthermore, the demonstration of the ability to modify one material by the selective CVI deposition of a second metal, exemplified by our Pd_{shell}−Au_{core}/TiO_2 CVI@SI material, using a simple and reproducible technique opens up many new possibilities in the preparation of "designer catalysts".

The catalytic data we present demonstrate the high activity of TiO_2-supported Pd-, Pt-, and Pd−Pt materials prepared by this new CVI methodology for both oxidation and hydrogenation reactions. We propose that the high catalytic performance reported is linked to the uniformly small particle size and "clean" nanoparticle and support surfaces obtained by the CVI route. We note that our titania-supported Pd/Pt materials can be utilized as a catalyst using a variety of aqueous and nonaqueous conditions and furthermore that they show major improvement when compared to other materials reported in the literature. For example, the low toluene selectivity in the oxidation of benzyl alcohol and the high benzoic acid selectivity in the oxidation of toluene we observed are markedly different from $AuPd/TiO_2$ catalysts[9,20,21,23] when used under similar conditions. Data we now report in the low-temperature oxidation of toluene using TBHP/air, in which TBHP is not acting as a stoichiometric oxidant, are also in contrast to data we obtained for sol-immobilized Pd−Pt/TiO_2 that displayed much lower catalytic activity[46] and other AuPd catalysts for which there was no apparent utilization of oxygen (from air)[23] as compared to the Pd−Pt/TiO_2 CVI material. These

findings point to the possibility of exploring low-temperature oxidation reactions involving C–H bonds using our new materials, and this idea can be extended to hydrogenation reactions, given that we accomplished quantitative levulinic acid hydrogenation to γ-valerolactone at 100 °C.

METHODS

Sample Preparation. For monometallic 2.5 wt % Pd/TiO_2 samples, TiO_2 (P25 Degussa, 0.98g) and palladium acetylacetonate, $Pd(acac)_2$, (Sigma-Aldrich 99 minimum%,72 mg) were placed into glass vial and mixed by manual shaking. This mixture was then transferred to a 50 mL Schlenk flask with a magnetic stirrer bar and the tube sealed. The tube was then evacuated at room temperature using a vacuum line (lowest pressure attainable was 10^{-3} mbar) followed by heating at 140 °C for 1 h under continuous vacuum conditions with stirring to accomplish sublimation and deposition of the organometallic precursor onto the support. The reaction vessel was then brought up to atmospheric pressure with air and the sample removed for further heat treatment. The color of the sample was light gray at this stage, indicating that some autoreduction of the Pd precursor had occurred. The as-prepared sample was loaded into a quartz or ceramic boat, placed into a horizontal furnace, and reduced in 5% H_2/Ar at 400 °C (ramp rate of 20 °C min^{-1}) for 3 h with a flow rate of 20 mL min^{-1} in order to fully pyrolyse the metal precursor.

Platinum acetylacetonate, Pt $(acac)_2$, was obtained from Sigma-Aldrich (99.9%) and used as the precursor in the preparation of Pt-containing catalysts. This same general procedure as described above was used to prepare 2.5 wt % Pt/TiO_2 (using 51 mg of $Pt(acac)_2$ and 0.98 g TiO_2) and 1.25 wt % Pt–1.25 wt % Pd/TiO_2 (using 17 mg $Pt(acac)_2$, 36 mg $Pd(acac)_2$, and 0.98g TiO_2) samples with the sublimation–deposition condition employed being 150 °C for 1 h under continuous vacuum. In the case of the bimetallic Pd–Pt sample, the metal precursors were mixed by manually shaking a glass sample vial containing the required amount of precursors prior to manual mixing with TiO_2. For the Pt-only material the sample was yellow after the sublimation–deposition step, whereas the Pt–Pd material was gray. These as-prepared materials were reduced in 5% H_2/Ar at 400 °C (ramp rate of 20 °C min^{-1}) for 3 h with a flow rate of 20 mL min^{-1}. Longer sublimation–deposition times or higher pyrolysis temperatures were found to lead to poorer catalytic performance, particularly for CO oxidation and benzyl alcohol oxidation. We determined that the preparation could quite easily be scaled up to 5-g batches using a larger Schlenk flask and appropriate stirring, as the catalytic performance (for toluene oxidation and levulinic acid hydrogenation) was not affected by the size of the manufactured batch.

Pd_{shell}–Au_{core}/TiO_2 catalysts were prepared by a hybrid CVI/sol-immobilization technique in the following manner. The sol-immobilization (SI) methodology was utilized for the preparation of Au/TiO_2 due to the small size of Au nanoparticles achieved in this method for which we have previously provided extensive characterization. In the case of Au, typical precursors for vapor deposition of Au are prohibitively expensive and require special handling. As such, we explored the concept of modifying a preformed Au material with a second metal, as outlined below, to demonstrate the versatility of our approach. 1 wt % Au/TiO_2 was prepared as previously reported using the SI methodology with water reflux treatment (90 °C, 1h) before drying to remove the PVA ligand shell.[29] $Pd(acac)_2$ (28.8 mg, 99.95% Sigma Aldrich) was added to the dried ground 1 wt % Au/TiO_2 (0.98g) in a sample vial and mixed by manual shaking. This was continued until it was observed that the yellow acetylacetonate powder was dispersed uniformly throughout the purple-colored Au material. The mixture was transferred to a Schlenk tube, and CVI synthesis was performed as outlined above for the Pd/Pt catalysts. The 'as-prepared' catalyst was light gray in color, and further treatment in 5% H_2/Ar (20 mL min^{-1}) for 3 h at 400 °C (20 °C min^{-1} ramp rate) was performed. The final color of the catalyst was dark gray. Prolonging treatment in H_2/Ar or the use of a 10% H_2/Ar reducing mixture (or higher % of H_2) led to a darker colored catalyst. If 50% H_2/Ar was used, the final material was black in color.

Structural Characterization. *Scanning Transmission Electron Microscopy.* Samples of catalysts were prepared for TEM/STEM analysis by dry dispersing the catalyst powder onto a holey carbon TEM grid. Phase contrast lattice imaging and high-angle annular dark-field (HAADF) imaging experiments were carried out using a 200 kV JEOL 2200FS scanning transmission electron microscope equipped with a CEOS aberration corrector. This microscope was also equipped with a Thermo-Noran X-ray energy dispersive spectroscopy (XEDS) system for compositional analysis.

X-ray Photoelectron Spectroscopy. X-ray photoelectron spectra were recorded on a Kratos Axis Ultra DLD spectrometer employing a monochromatic AlK_α X-ray source (75–150 W) and analyzer pass energies of 160 eV (for survey scans) or 40 eV (for detailed scans). Samples were mounted using double-sided adhesive tape and binding energies referenced to the C(1s) binding energy of adventitious carbon contamination which was taken to be 284.7 eV.

Elemental Analysis. Carbon–hydrogen–nitrogen (CHN) analysis and ICP-MS were provided by Warwick Analytical Services (UK). Samples were measured in duplicate.

Catalyst Testing. *CO Oxidation.* Catalyst samples were evaluated for CO oxidation using a fixed-bed laboratory microreactor operated at atmospheric pressure. Typically CO (0.5% in synthetic air) was fed to the reactor at a controlled rate of 21 mL min^{-1}, using mass flow controllers and passed over the catalyst (50 mg). The catalyst temperature was maintained at 25 or 50 °C by immersing the quartz bed in a thermostatically controlled water bath. The products were analyzed using online gas chromatography with a 1.5 m packed carbosieve column and thermal conductivity detector. These conditions are equivalent to a total gas space velocity (GHSV) of 25,200 h^{-1}.

Hydrocarbon Oxidation in Autoclave Reactors. The oxidation reactions were carried out in a stirred reactor (100 mL, Parr reactor). The vessel was charged with the desired substrate (10–40 mL) and catalyst (0.05–0.2 g). The autoclave was then purged five times with oxygen, leaving the vessel at 150 psi pressure. The stirrer was set at 1500 rpm, and the reaction mixture was raised to the required temperature (120 °C for benzyl alcohol oxidation and 160 °C for toluene oxidation). Samples from the reactor were taken periodically, *via* a sampling system. For the identification and analysis of the products, a GC–MS and GC (a Varian Star 3400 cx with a 30 m CP-Wax 52 CB column) were employed. In addition, the products were identified by comparison with commercially pure 'standard' samples. For the quantification of the amounts of reactants consumed and products generated, the external calibration method was used.

Hydrocarbon Oxidation in Glass Reactors. All reactions were performed in a stirred, glass, round-bottom flask (100 mL) fitted with a reflux condenser and heated in an oil bath. Typically, the hydrocarbon (toluene, 10 mL) and the desired amount of catalyst were suspended in the solution. Then *tert*-butyl hydrogen peroxide (TBHP 1:1 ratio with toluene) was added and the mixture reacted at 80 °C in an air atmosphere. The reactions were typically carried out for timespans between 0.5 and 96 h.

Hydrogenation of Levulinic Acid. The catalyst (50 mg) was charged into a 50 mL Parr autoclave fitted with a PTFE liner (internal volume 35 mL). Aqueous levulinic acid (98% Sigma-Aldrich, 10 wt %, 10 mL) was added to the reactor followed by purging sequentially with N_2 and then H_2 (three times each). The reactor was then charged with pure H_2 (usually 30 bar) and heated to the desired reaction temperature with continuous stirring (1200 rpm). The reaction was carried out for the desired time and the reactor then cooled to below 10 °C with ice. The

gas-phase product was collected in a gas bag, while the liquid-phase product was filtered using a 10 mL plastic syringe fitted with glass filter paper at its base. The gas and liquid phases were analyzed by GC-FID on a Varian 450-GC fitted with a CP-Sil 5CB capillary column (50 m length, 0.32 mm ID). The GC was fitted with a methaniser unit (particularly useful for CO/CO_2 analysis of the gas phase), and gaseous products were identified and quantified against a calibration curve generated from commercial standards where possible (*i.e.*, BOC gases). The liquid-phase products were identified and quantified by calibration against authentic standards (Sigma-Aldrich) and also by GC–MS as described in our analysis of the products of benzyl alcohol oxidation.

Conflict of Interest: The authors declare no competing financial interest.

Supporting Information Available: Additional catalytic data and comparisons, catalyst characterization and product analysis data. This material is available free of charge via the Internet at http://pubs.acs.org.

REFERENCES AND NOTES

1. Bond, G. C.; Thompson, D. T. Catalysis by Gold. *Catal. Rev. Sci. Eng.* **1999**, *41*, 319–388.
2. Campbell, C. T.; Parker, S. C.; Starr, D. E. The Effect of Size-Dependent Nanoparticle Energetics on Catalyst Sintering. *Science* **2002**, *298*, 811–814.
3. Valden, M.; Lai, X.; Goodman, D. W. Onset of Catalytic Activity of Gold Clusters on Titania with the Appearance of Nonmetallic Properties. *Science* **1998**, *281*, 1647–1650.
4. Schwarz, J. A.; Contescu, C.; Contescu, A. Methods for Preparation of Catalytic Materials. *Chem. Rev.* **1995**, *95*, 477–510.
5. Campelo, J. M.; Luna, D.; Luque, R.; Marinas, J. M.; Romero, A. A. Sustainable Preparation of Supported Metal Nanoparticles and Their Applications in Catalysis. *ChemSusChem* **2009**, *2*, 18–45.
6. Liu, Y.; Chi, M. F.; Mazumder, V.; More, K. L.; Soled, S.; Henao, J. D.; Sun, S. H. Composition-Controlled Synthesis of Bimetallic PdPt Nanoparticles and Their Electro-Oxidation of Methanol. *Chem. Mater.* **2011**, *23*, 4199–4203.
7. Wang, L.; Nemoto, Y.; Yamauchi, Y. Direct Synthesis of Spatially-Controlled Pt-On-Pd Bimetallic Nanodendrites with Superior Electrocatalytic Activity. *J. Am. Chem. Soc.* **2011**, *133*, 9674–9677.
8. Xia, Y.; Xiong, Y.; Lim, B.; Skrabalak, S. E. Shape-Controlled Synthesis of Metal Nanocrystals: Simple Chemistry Meets Complex Physics?. *Angew. Chem. Int. Ed* **2009**, *48*, 60–103.
9. Kesavan, L.; Tiruvalam, R.; Ab Rahim, M. H.; Bin-Saiman, M. I.; Enache, D. I.; Jenkins, R. L.; Dimitratos, N.; Lopez-Sanchez, J. A.; Taylor, S. H.; Knight, D. W.; *et al.* Solvent-Free Oxidation of Primary Carbon-Hydrogen Bonds in Toluene Using Au-Pd Alloy Nanoparticles. *Science* **2011**, *331*, 195–199.
10. Serp, P.; Feurer, R.; Morancho, R.; Kalck, P. One-Step Preparation of Highly Dispersed Supported Rhodium Catalysts by Low-Temperature Organometallic Chemical Vapour Deposition. *J. Catal.* **1995**, *157*, 294–300.
11. Serp, P.; Klack, P.; Feurer, R. Chemical Vapor Deposition Methods for the Controlled Preparation of Supported Catalytic Materials. *Chem. Rev.* **2002**, *102*, 3085–3128.
12. Gozum, J. E.; Pollina, D. M.; Jensen, J. A.; Girolami, G. S. "Tailored" Organometallics as Precursors for the Chemical Vapor Deposition of High-Purity Palladium and Platinum Thin Films. *J. Am. Chem. Soc.* **1988**, *110*, 2688–2689.
13. Haruta, M.; Kobayashi, T.; Sano, H.; Yamada, N. Novel Gold Catalysts for the Oxidation of Carbon Monoxide at a Temperature Far Below 0 °C. *Chem. Lett.* **1987**, *16*, 405–408.
14. Okumura, M.; Nakamura, S.; Tsubota, S.; Nakamura, T.; Azuma, M.; Haruta, M. Chemical Vapor Deposition of Gold on Al_2O_3, SiO_2, and TiO_2 for the Oxidation of CO and of H_2. *Catal. Lett.* **1998**, *51*, 53–58.
15. Santo, V. D.; Mondelli, C.; Grandi, V. D.; Gallo, A.; Recchia, S.; Sordelli, L.; Psaro, R. Supported Rh Catalysts for Methane Partial Oxidation Prepared by OM-CVD of $Rh(Acac)(CO)_2$. *App. Catal. A* **2008**, *34*, 126–133.
16. Caussat, B.; Vahlas, C. CVD and Powders: A Great Potential to Create New Materials. *Chem. Vap. Deposition* **2007**, *13*, 443–445.
17. Gallo, A.; Tiozzo, C.; Psaro, R.; Carniato, F.; Guidotti, M. Niobium Metallocenes Deposited onto Mesoporous Silica *via* Dry Impregnation as Catalysts for Selective Epoxidation of Alkenes. *J. Catal.* **2013**, *298*, 77–83.
18. Papandrew, A. B.; Chisholm, C. R.I.; Elgammal, R. A.; Özer, M. M.; Zecevic, S. K. Advanced Electrodes for Solid Acid Fuel Cells by Platinum Deposition on CsH_2PO_4. *Chem. Mater.* **2011**, *23*, 1659–1667.
19. Forde, M. M.; Armstrong, R. D.; Hammond, C.; He, Q.; Jenkins, R. L.; Kondrat, S. A.; Dimitratos, N.; Lopez-Sanchez, J. A.; Taylor, S. H.; Willock, D.; *et al.* Partial Oxidation of Ethane to Oxygenates Using Fe- and Cu-Containing ZSM-5. *J. Am. Chem. Soc.* **2013**, *135*, 11087–11099.
20. Lopez-Sanchez, J. A.; Dimitratos, N.; Miedziak, P.; Ntainjua, E.; Edwards, J. K.; Morgan, D.; Carley, A. F.; Tiruvalam, R.; Kiely, C. J.; Hutchings, G. J. Au-Pd Supported Nanocrystals Prepared by a Sol Immobilisation Technique as Catalysts for Selective Chemical Synthesis. *Phys. Chem. Chem. Phys.* **2008**, *10*, 1921–1930.
21. Dimitratos, N.; Lopez-Sanchez, J. A.; Morgan, D.; Carley, A. F.; Tiruvalam, R.; Kiely, C. J.; Bethell, D.; Hutchings, G. J. Solvent-Free Oxidation of Benzyl Alcohol Using Au-Pd Catalysts Prepared by Sol Immobilisation. *Phys. Chem. Chem. Phys.* **2009**, *11*, 5142–5153.
22. Enache, D. I.; Edwards, J. K.; Solsona-Espriu, P. L. B.; Carley, A. F.; Herzing, A. A.; Watanabe, M.; Kiely, C. J.; Knight, D. W.; Hutchings, G. J. Solvent-Free Oxidation of Primary Alcohols to Aldehydes Using Au-Pd/ TiO_2 Catalysts. *Science* **2006**, *311*, 362–365.
23. Bin-Saiman, M. I.; Brett, G. L.; Tiruvalam, R.; Forde, M. M.; Sharples, K.; Thetford, A.; Jenkins, R. L.; Dimitratos, N.; Lopez-Sanchez, J. A.; Murphy, D. M.; *et al.* Involvement of Surface-Bound Radicals in the Oxidation of Toluene Using Supported Au-Pd Nanoparticles. *Angew. Chem. Int. Ed* **2012**, *51*, 5981–5985.
24. Bozell, J. J.; Moens, L.; Elliott, D. C.; Wang, Y.; Neuenscwander, G. G.; Fitzpatrick, S. W.; Bilski, R. J.; Jarnefeld, J. L. Production of Levulinic Acid and Use as a Platform Chemical for Derived Products. *Resour. Conserv. Recycl.* **2000**, *28*, 227–239.
25. Bozell, J. J. Connecting Biomass and Petroleum Processing with a Chemical Bridge. *Science* **2010**, *329*, 522–523.
26. Alonso, D. M.; Bond, J. Q.; Dumesic, J. A. Catalytic Conversion of Biomass to Biofuels. *Green Chem.* **2010**, *12*, 1493–1513.
27. Alonso, D. M.; Wettstein, S. G.; Dumesic, J. A. Bimetallic Catalysts for Upgrading of Biomass to Fuels and Chemicals. *Chem. Soc. Rev.* **2012**, *41*, 8075–7098.
28. Sivakumar, P.; Ishak, R.; Tricoli, V. Novel Pt–Ru Nanoparticles Formed by Vapour Deposition as Efficient Electrocatalyst for Methanol Oxidation Part I. Preparation and Physical Characterization. *Electrochim. Acta* **2005**, *50*, 3312–3319.
29. Lopez-Sanchez, J. A.; Dimitratos, N.; Hammond, C.; Brett, G. L.; Kesavan, L.; White, S.; Miedziak, P.; Tiruvalam, R.; Jenkins, R. L.; Carley, A. F.; *et al.* Facile Removal of Stabilizer-Ligands from Supported Gold Nanoparticles. *Nat. Chem.* **2011**, *3*, 550–556.
30. Chaudhuri, R. G.; Paria, S. Core/Shell Nanoparticles: Classes, Properties, Synthesis Mechanisms, Characterization, and Applications. *Chem. Rev.* **2011**, *112*, 2373–2433.
31. Yin, A.-X.; Min, X.-Q.; Zhang, Y.-W.; Yan, C.-H. Shape-Selective Synthesis and Facet-Dependent Enhanced Electrocatalytic Activity and Durability of Monodisperse Sub-10 nm Pt-Pd Tetrahedrons and Cubes. *J. Am. Chem. Soc.* **2011**, *113*, 3816–3819.
32. Kang, S. W.; Lee, Y. W.; Park, Y.; Choi, B.-S.; Hong, J. W.; Park, K.-H.; Han, S. W. One-Pot Synthesis of Trimetallic Au@PdPt Core Shell Nanoparticles with High Catalytic Performance. *ACS Nano* **2013**, *7*, 7945–7955.
33. Oezaslan, M.; Hasché, F.; Strass, P. Pt-Based Core-Shell Catalyst Architectures for Oxygen Fuel Cell Electrodes. *J. Phys. Chem. Lett.* **2013**, *4*, 3273–3291.

34. Comotti, M.; Li, W.-C; Spliethoff, B.; Schüth, F. Support Effect in High Activity Gold Catalysts for CO Oxidation. *J. Am. Chem. Soc.* **2006**, *128*, 917–924.
35. Konova, P.; Naydenov, A.; Venkov, C.; Mehandjiev, D.; Andreeva, D.; Tabakova, T. Activity and Deactivation of Au/TiO_2 Catalyst in CO Oxidation. *J. Mol. Catal. A* **2004**, *213*, 235–240.
36. Moreau, F.; Bond, G. C. CO Oxidation Activity of Gold Catalysts Supported on Various Oxides and Their Improvement by Inclusion of an Iron Component. *Catal. Today* **2006**, *114*, 362–368.
37. Liu, L.; Zhou, F.; Wang, L.; Qi, X.; Shi, F.; Deng, Y. Low-Temperature CO Oxidation over Supported Pt, Pd Catalysts: Particular Role of FeO_x Support for Oxygen Supply During Reactions. *J. Catal.* **2010**, *274*, 1–10.
38. Li, S.; Liu, G.; Lian, H.; Jia, M.; Zhao, G.; Jiang, D.; Zhang, W. Low-Temperature CO Oxidation over Supported Pt Catalysts Prepared by Colloid-Deposition Method. *Catal. Commun.* **2008**, *9*, 1045–1049.
39. Ebbesen, S. D.; Mojet, B. L.; Lefferts, L. *In Situ* ATR-IR Study of CO Adsorption and Oxidation over Pt/Al_2O_3 in Gas and Aqueous Phase: Promotion Effects by Water and pH. *J. Catal.* **2007**, *246*, 66–73.
40. Siani, A.; Alexeev, O. S.; Captain, B.; Lafaye, G. M.; Patrice; Adams, R. D.; Amiridis, M. D. Synthesis of Cluster-Derived $PtFe/SiO_2$ Catalysts for the Oxidation of CO. *J. Catal.* **2008**, *255*, 162–176.
41. Seo, P. W.; Choi, H. J.; Hong, S. I.; Hong, S. C. A Study on the Characteristics of CO Oxidation at Room Temperature by Metallic Pt. *J. Haz. Mater.* **2010**, *178*, 917–925.
42. Yoon, K.; Yang, Y.; Lu, P.; Wan, D.; Peng, H.-C.; Masias, K. S.; Fanson, P. T.; Campbell, C. T.; Xia, Y. A Highly Reactive and Sinter-Resistant Catalytic System Based on Platinum Nanoparticles Embedded in the Inner Surfaces of CeO_2 Hollow Fibers. *Angew. Chem. Int. Ed* **2012**, *51*, 9543–9546.
43. Enache, D. I.; Barker, D.; Edwards, J. K.; Taylor, S. H.; Knight, D. W.; Carley, A. F.; Hutchings, G. J. Solvent-Free Oxidation of Benzyl Alcohol Using Titania-Supported Gold−Palladium Catalysts: Effect of Au−Pd Ratio on Catalytic Performance. *Catal. Today* **2007**, *122*, 407–411.
44. He, Q.; Miedziak, P. J.; Kesavan, L.; Dimitratos, N.; Sankar, M.; Lopez-Sanchez, J. A.; Edwards, J. K.; Forde, M. M.; Knight, D. W.; Taylor, S.; *et al.* Switching-Off Toluene Formation in the Solvent-Free Oxidation of Benzyl Alcohol Using Supported Trimetallic Au−Pd−Pt Nanoparticles. *Faraday Discuss.* **2013**, *162*, 365–378.
45. Luo, Y. R. In *CRC Handbook of Chemistry and Physics 1999−2000: A Ready-Reference Book of Chemical and Physical Data*, 90th ed.; Lide, D. R., Ed. CRC Press: Boca Raton, 2009; pp 9−67.
46. Peneau, V.; He, Q.; Shaw, G.; Kondrat, S. A.; Davies, T. E.; Miedziak, P.; Forde, M. M.; Dimitratos, N.; Kiely, C. J.; Hutchings, G. J. Selective Catalytic Oxidation Using Supported Gold−Platinum and Palladium−Platinum Nanoalloys Prepared by Sol-Immobilisation. *Phys. Chem. Chem. Phys.* **2013**, *15*, 10636–10644.
47. Sosnovsky, G.; Rawlinson, D. J., Chemistry of Hydroperoxides in the Presence of Metal Ions. In *Organic Peroxides*; Swern, D., Ed.; Wiley: New York, 1971; Vol. 2, pp 159−165.
48. Lange, J.-P.; Price, R.; Ayoub, P. M.; Louis, J.; Petrus, L.; Clarke, L.; Gosselink, H. Valeric Biofuels: A Platform of Cellulosic Transportation Fuels. *Angew. Chem., Int. Ed.* **2010**, *49*, 4479–4483.
49. Schuette, H. A.; Thomas, R. W. Normal Valerolactone. 111. Its Preparation by the Catalytic Reduction of Levulinic Acid with Hydrogen in the Presence of Platinum Oxide. *J. Am. Chem. Soc.* **1930**, *52*, 3010–3012.
50. Christian, R. V., Jr.; Brown, H. D.; Hixon, R. M. Derivatives of γ-Valerolactone, 1,4-Pentanediol, and 1,4-Di-(β-cyanoethoxy)-pentane. *J. Am. Chem. Soc.* **1947**, *69*, 1961–1963.